Polarized neutron reflectometry of a patterned magnetic film with a ^{3}He analyzer and a position-sensitive detector

W. C. Chen[a] and T. R. Gentile
NIST, 100 Bureau Drive, MS 8461, Gaithersburg, Maryland 20899

K. V. O'Donovan, J. A. Borchers, and C. F. Majkrzak
NIST, 100 Bureau Drive, MS 8562, Gaithersburg, Maryland 20899

(Received 15 March 2004; accepted 9 July 2004; published 20 September 2004)

We have employed a polarized ^{3}He spin filter in conjunction with a position-sensitive detector (PSD) to perform efficient polarization analysis of neutron diffuse reflectivity. This work was carried out on the NG-1 polarized neutron reflectometer at the National Institute of Standards and Technology Center for Neutron Research. We measured the specular and diffuse reflectivity of a patterned magnetic array that has periodic square holes in a Co film. Analysis of the data yielded spin-analyzed two-dimensional $Q_x - Q_z$ reciprocal space maps for the sample in magnetized and demagnetized states. We compared the measurements obtained with a ^{3}He analyzer and a PSD with those obtained using a conventional supermirror analyzer and a ^{3}He proportional counter. The results are in good agreement. For this experiment, ^{3}He gas was polarized by the spin-exchange optical pumping method and stored in a uniform magnetic field provided by a shielded solenoid. Improved optical pumping using a spectrally narrowed diode laser array yielded an initial ^{3}He polarization of 70% in a ^{3}He cell volume of 280 cm^3. © *2004 American Institute of Physics.* [DOI: 10.1063/1.1791312]

I. INTRODUCTION

Improved fabrication techniques for magnetic thin films has motivated construction of smaller magnetic devices such as recording media and sensors, making analysis techniques that characterize the magnetic features in such materials essential. Among these materials and technologies, patterned magnetic arrays have recently attracted considerable attention because of their promising advantages for high-density data storage and sensor applications.[1,2] Moreover, they are ideally suited for studying fundamental magnetic interactions due mainly to their highly controllable structures. As demonstrated a decade ago,[3] specular and diffuse polarized neutron reflectometry (PNR) is a powerful probe to obtain information on the depth profile of the magnetization, in-plane domains, and interfacial roughness of magnetic thin films.[4] PNR is especially important for buried magnetic films because other techniques such as scanning electron microscopy with polarization analysis and magnetic force microscopy can only probe the magnetic structures at or near the surface.

PNR has typically employed supermirrors (SM) for polarization analysis due to their high efficiency and neutron transmission.[5,6] While a single supermirror analyzer is well matched to specular PNR and thus available on most reflectometers, its limited angular acceptance makes it inefficient for diffusely reflected beams. One possible solution that still utilizes the supermirror technology is to use a stack of curved or bent supermirrors.[7,8] These devices do have a larger angular acceptance of a few degrees. However, in some situations an angular-dependent transmission due to the bender focusing properties has to be taken into account. The other consideration when using the beam reflected from a supermirror bender is that the beam could be more divergent due to the curvature. Polarized ^{3}He analyzers, which rely on the strong spin dependence of the neutron absorption cross section for ^{3}He gas, are in principle suitable for any divergent scattered beam. This capability has been employed for small-angle neutron scattering (SANS),[9] diffuse reflectometry,[10,11] and large solid angle polarization analysis at thermal neutron wavelengths.[12] In general, a ^{3}He cell could be made large enough to avoid restricting the angular acceptance. In addition, a ^{3}He spin filter can have a homogeneous analyzing efficiency, predictable analyzing efficiency and transmission, negligible small angle scattering from the ^{3}He cell, and low gamma-ray background. By measuring the data from the position-sensitive detector (PSD) at different sample angles, a polarized ^{3}He analyzer in conjunction with a linear PSD provides a two-dimensional map of the wave vector transfer in reciprocal space. These features of the ^{3}He analyzer are important for measurements of weak off-specular scattering.

Off-specular scattering has many possible origins. It typically arises from lateral structural and magnetic correlations such as magnetic domains, surface and interface roughness (both structural and magnetic), structural grains, and artificially patterned structures. These structural and magnetic features might be laterally correlated or uncorrelated, resulting in a different off-specular pattern. The length scales of lateral inhomogeneities such as atomic interlayer interdiffusion, steps, and waviness accessible by PNR vary from

[a]Author to whom correspondence should be addressed; electronic mail: wcchen@nist.gov

$\sim 0.1\ \mu$m to $\approx 40\ \mu$m. Structurally induced off-specular scattering has been discussed and measured using diffuse x-ray and neutron scattering.[13,14] Magnetically induced off-specular scattering has been discussed[15] and measured using polarized diffuse neutron reflectometry.[16,17]

Two optical pumping methods are currently in use for producing polarized ^{3}He gas for neutron spin filters, metastability-exchange optical pumping (MEOP),[18] and spin-exchange optical pumping (SEOP).[19] For spin filters in which the gas is not continuously optically pumped, both high ^{3}He polarization and a long polarization relaxation time are important for their performance in neutron scattering applications. For the SEOP method, we have made significant progress in these two aspects. Our recent success in fabricating cells with relaxation times of several hundred hours[20] and producing ^{3}He gas with 75% ^{3}He polarization[21] have improved the performance of polarized ^{3}He spin filters for applications in polarized neutron scattering. In addition, this method is well suited for future continuous operation on neutron beam lines.

Recently, we have tested a ^{3}He spin filter on the NIST Center of Neutron Research (NCNR) NG-1 polarized neutron reflectometer by performing polarization analysis of the specular reflection from an epitaxial magnetic bilayer, $Mn_{0.52}Pd_{0.48}/Fe$.[22] Here we report the use of a more efficient ^{3}He analyzer in conjunction with a PSD and demonstrate its application for diffuse scattering measurements of a patterned magnetic thin film on the NCNR NG-1 reflectometer.

II. POLARIZED ^{3}He SPIN FILTER AS A SPIN ANALYSIS DEVICE

A. Principles of ^{3}He spin filters

Neutron spin filters based on transmission through polarized ^{3}He gas rely on the strong spin dependence of the neutron absorption cross section for ^{3}He gas via the resonance reaction $^3\mathrm{He}(n,p)^3\mathrm{H}$. The dependence of the analyzing efficiency and neutron transmission on ^{3}He polarization and other parameters such as the neutron wavelength, the ^{3}He gas density, and the cell length is discussed elsewhere.[22] For the SEOP method, the laser power needed is proportional to the cell volume. Spectrally narrowing the laser light substantially decreases the power requirement[23] and permits higher ^{3}He polarization in large cells.[21] Nevertheless, the achievable ^{3}He polarization is currently limited to $1/(1+X)$, where X accounts for the recent observation that the ^{3}He relaxation rate increases linearly with the Rb vapor density with a slope that exceeds the Rb–^{3}He spin-exchange rate constant.[21,24] X varies from cell to cell but is typically about 0.33, which limits the maximum ^{3}He polarization to 75%. We now routinely obtain ^{3}He polarizations of 74%–77% for long relaxation time ^{3}He cells with volumes up to 500 cm^3. To obtain higher ^{3}He polarization using SEOP, the source of temperature-dependent relaxation must be eliminated or reduced. Studies are under way at the National Institute of Standards and Technology (NIST) and the University of Wisconsin at Madison.

For the 280 cm^3 cell with a relaxation time of 520 h, "Bullwinkle," used in this experiment, we have obtained 64% ^{3}He polarization with a single 20 W spectrally narrowed diode laser. For this work, the addition of an available 30 W broadband laser and a longer optical pumping time allowed us to reach 70.5% ^{3}He polarization. The ^{3}He cell was polarized off line in a 2.6 mT magnetic field and transported to the reflectometer in a 1.3 mT field provided by a portable solenoid.

B. Uniformity of the analyzing power of the ^{3}He spin filter

To maintain the polarization of the ^{3}He cell while in use on the reflectometer, the cell was positioned in the center of a short shielded solenoid (SSS), which consists of a solenoid surrounded by cylindrical mu-metal shielding and mu-metal end caps. The SSS is 27 cm in diameter and 30 cm long and each end cap has a 5-cm-diam hole to pass the neutron beam. We surrounded the hole nearest the PSD with neutron shielding material to prevent transmission of the beam through the mu-metal. Prior to our experiments, we first determined if a polarized beam could be efficiently transmitted through the solenoid. We placed the SSS only (no cell) on the sample stage to allow for translation (± 1.4 cm) and rotation ($\pm 5°$) in the horizontal plane (scattering plane). The polarization of neutrons was maintained by a guide field perpendicular to the scattering plane along the entire neutron flight path except the region of the SSS. As a neutron enters the SSS, its spin is adiabatically rotated to be along the magnetic field in the SSS, which is parallel to the neutron beam. When a neutron exits the SSS, its spin is adiabatically rotated back to be along the vertical guide field. The field strength in the SSS needed to maintain the ^{3}He polarization is fairly arbitrary, but heat dissipation becomes significant at fields above about 6 mT. We operated at a field of 5 mT, which provided sufficient leakage of longitudinal field for efficient adiabatic rotation of the neutron spin. We used a Fe/Si SM polarizer and a precession coil spin flipper[25] in the incident beam to select the polarization of the incident neutrons. The polarization of the neutrons transmitted through the SSS was determined using a second precession coil spin flipper and a SM analyzer. For different trajectories of the main beam through the solenoid, we measured all four spin-dependent transmissions T^{++}, T^{+-}, T^{-+}, and T^{--}, where the first (second) index refers to the initial (final) neutron spin state and the "+" ("−") symbol corresponds to the up (down) state of the neutron. We define the front (rear) instrumental flipping ratio as $F_f = T^{++}/T^{-+}$ ($F_r = T^{++}/T^{+-}$). Figure 1 shows the front transmission asymmetry A_f, which is related to the flipping ratio by $A_f = (F_f - 1)/(F_f + 1)$, as a function of the translation and the rotation angle of the SSS. The front and rear (not shown) transmission asymmetries were found to be reduced by no more than 3% and 7% respectively, with a more substantial drop occurring only for a small range of extreme trajectories. This indicates depolarization is not an issue until neutrons pass very close to the end cap holes. The difference between the front and rear transmission asymmetries may be due to a difference in the field homogeneity around the two flippers.

The uniformity of the analyzing efficiency of the ^{3}He spin filter is determined primarily by the uniformity of the gas thickness of the blown glass cell. For the Bullwinkle cell,

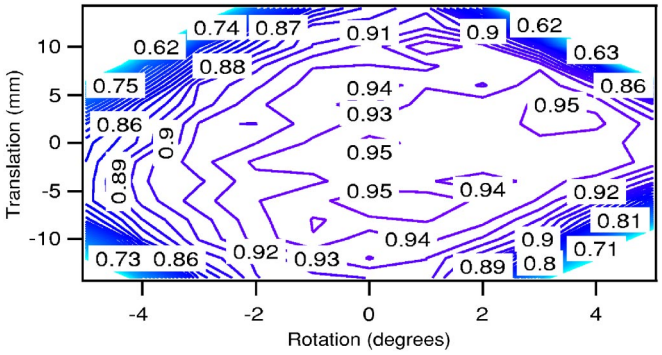

FIG. 1. (Color online) Contour plot of the front transmission asymmetry A_f as a function of the translation and the rotation angle of the SSS. The SSS was located in the sample position and no ^{3}He cell was in the SSS. This shows that neutron depolarization is not an issue until neutrons pass very close to the end cap holes.

we found that the gas path length varies by ±3% over the useful area of the cell, which results in only a ±1% variation in the analyzing efficiency.

C. Small-angle scattering of the ^{3}He cell

The spin filter cell is made from GE180[26] glass, which is boron free and has low permeability to ^{3}He gas. Although quartz has been used for SEOP, it is not ideal because of gas loss in long-term use at the typical temperatures used for SEOP. In addition, we have reliably obtained very long relaxation times with GE180 glass. Small-angle scattering from the cell, if observable, would be superimposed on the weak diffuse scattering from the sample. We measured the small-angle neutron scattering signal from a ^{3}He cell on the NG-7 SANS instrument at the NCNR, using a quasimonochromatic beam with a center wavelength of 0.6 nm and a full width at half maximum (FWHM) of 0.07 nm.[27] (The cell tested is similar in geometry to the Bullwinkle cell, but filled with a pressure of only 1.3 mbar.) The measured SANS on an absolute scale (i.e, the macroscopic differential scattering cross section) was almost constant in the measured Q range of $0.1-3$ nm^{-1}, indicating that there is no structure-induced small-angle scattering from the cell. The measured scattering of 0.016 sr^{-1} is consistent with the measured attenuation of the neutron beam by the cell, assuming isotropic scattering. We have measured an attenuation length of 55 mm±5 mm for GE180 glass at a wavelength of 0.495 nm. The measured neutron transmission through a GE180 cell is typically 0.88, corresponding to a total glass thickness of 7 mm.

We also measured the small-angle scattering over a range of ±3° around the beam axis with and without this test cell at the sample position of the NG-1 reflectometer. After correcting for cell transmission, the intensity difference between these measurements yields the small-angle scattering from the ^{3}He cell itself. We did not see any observable difference between measurements with and without the cell, hence scattering from the cell contributes a negligible background in these experiments.

D. Time dependence of the ^{3}He polarization

During our reflectivity experiments, the polarized ^{3}He gas was not continuously optically pumped, hence the analyzing efficiency and transmission of the ^{3}He analyzer decreased with time due to an exponential decay of the ^{3}He polarization. To determine the rate of decay for subsequent data corrections, we measured the unpolarized neutron transmission of the polarized ^{3}He cell at regular time intervals with the SM polarizer and the sample out of the beam. At the end of the experiment, we measured the neutron transmission of the depolarized ^{3}He cell and extracted the ^{3}He polarization as a function of time.[28] During the course of the 65 h experiment, the ^{3}He polarization decayed from 70.5% to 50.2%, corresponding to a decrease in ^{3}He analyzing efficiency from 0.972 (flipping ratio of 71) to 0.904 (flipping ratio of 20), and a decrease in transmission of the desired spin state from 36.5% to 20.2%. An exponential fit to the ^{3}He polarization yielded a relaxation time of 195 h±4 h. The relaxation time of the ^{3}He gas in the Bullwinkle cell has previously been measured by nuclear magnetic resonance[20] to be 520 h, which is dominated by dipole–dipole relaxation.[29] However, in the SSS there is additional relaxation due to a magnetic field gradient.[30] In both earlier off-line tests and a previous NG-1 experiment[22] we had observed a relaxation time of 350 h in the SSS, which was consistent with a measured gradient of 3×10^{-4} cm^{-1} in the magnetic field. The lower value of 195 h observed in this experiment may be due to gradients produced by guide fields that were improvised to maintain the polarization of the neutron beam. We are currently constructing a new shielded solenoid with the goal of obtaining relaxation times that are not limited by field gradients.

The relaxation time in the SSS was optimized off line by mapping the field and by measuring the relaxation of low pressure cells. At a pressure of 1.3 mbar, the relaxation rate due to magnetic field gradients is 1000 times faster than in the Bullwinkle cell, allowing relaxation tests to be performed on a relatively short time scale. The low pressure cells are optically pumped using a compact MEOP apparatus that employs a low power diode laser[31] and a static polarimeter.[32] Although the magnetic shield almost completely avoids the need for compensating coils on the ends of the short solenoid, we found that seven turns were still necessary. After demagnetizing the shield and optimizing the number of compensation coils, we measured a relaxation time of 350 h for the Bullwinkle cell, which is still lower than what should be possible for the SSS. Field maps suggest that spatial inhomogeneity in the magnetic shielding material or asymmetry in the solenoid-end cap separation may be the limiting factor.

III. NIST NG-1 REFLECTOMETER CONFIGURATION

A. Conventional supermirror polarizer and analyzer

In the standard configuration of the NG-1 reflectometer shown in Fig. 2(b),[33] a monochromatic neutron beam with a wavelength of 0.475 nm and a resolution ($\Delta\lambda/\lambda$) of 1.5% is provided by reflection from a pyrolytic graphite monochromator. After the neutrons are incident upon a Fe/Se super-

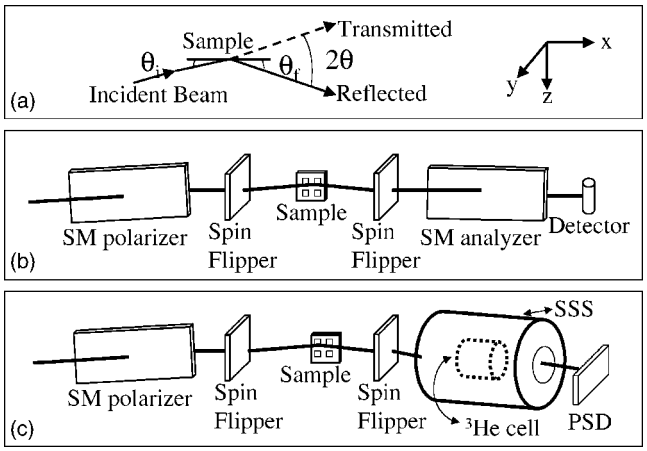

FIG. 2. Schematic diagrams of the NG-1 reflectometer at the NIST NCNR: (a) a plane view of the scattering geometry; (b) conventional SM analyzer configuration; (c) ^{3}He/PSD configuration. The ^{3}He analyzer and PSD were mounted on the same arm of the instrument as the pencil detector. Collimating slits (not shown) were used in the conventional configuration, but were not used after the sample in the ^{3}He/PSD system. The sample and guide field are vertical (along the *y* axis) except for the field in the SSS, which is along the neutron beam.

mirror and pass through a precession coil spin flipper, the neutron flux at the sample location is typically 1.3×10^4 cm^{-2} s^{-1}. The neutrons scattered from the sample pass through a second spin flipper, reflect from a supermirror analyzer, and are detected by a 2.5 cm diameter ^{3}He proportional counter, which we will refer to as the "pencil" detector. The neutron polarization is maintained by a guide field perpendicular to the scattering plane along the entire neutron flight path. The polarizing efficiencies of the two supermirrors are typically about 98% and the efficiencies of the spin flippers are above 97%.

In a reflectivity experiment, the neutrons are incident upon the sample surface at an angle θ_i and scattered at an angle θ_f as shown in Fig. 2(a). For scans with the pencil detector, the sample can be rotated to vary θ_i and the angle of the detector arm can be moved to vary $2\theta = \theta_i + \theta_f$. The specular reflectivity is measured by varying θ_i and 2θ together in a 1:2 ratio (ie., $2\theta = 2\theta_i$). The off-specular reflectivity is typically sampled by scanning θ_i at a fixed value of 2θ (i.e., rocking curve) or by scanning 2θ at a fixed value of θ_i. Thorough characterization of the off-specular scattering is time consuming and requires, for example, a series of rocking curves at different values of 2θ.

B. ^{3}He analyzer and PSD

For our demonstration experiments described here, the ^{3}He analyzer and PSD were used in lieu of the supermirror analyzer and pencil detector, respectively. The ^{3}He/PSD system was mounted on the same arm as the pencil detector with an offset in 2θ of 18°. As schematically shown in Fig. 2(c), the supermirror analyzer was removed when the ^{3}He analyzer was used to avoid possible effects of strong magnetic fields on the ^{3}He spin filter. The neutron polarization was maintained by a vertical guide field along the entire neutron flight path, except where the neutron spin is adiabatically rotated to be along the field in the SSS as discussed in Sec. II B. The distance between the sample and the center of the 12-cm-wide, 5-cm-high, 256 pixel PSD was 123 cm. Using a piece of tape that exhibits strong, isotropic scattering, we measured the overall efficiency of the PSD relative to the pencil detector to be 70% ± 9%. During our experiment with the ^{3}He analyzer, the efficiency of approximately 50 pixels near each edge was reduced due to shadowing by the circular hole in the end caps of the SSS.

For a fixed value of incident scattering angle θ_i, the PSD detects the neutrons scattered over a range of 2θ values. The specular and off-specular scattering can thus be measured simultaneously over a wide angular range by scanning θ_i. Interpretation of the PSD data requires a precise calibration of the angular position of each pixel. Using an unpolarized beam to calibrate the PSD, we scanned the PSD through the Bragg positions of the first and third order superlattice peaks for a $[Fe/W]_{30}$ multilayer with a bilayer thickness of 7.5 nm.[34] For each of the superlattice peaks, we fit the intensity profile (intensity vs pixel) to a Gaussian for each angular position of the PSD. We then obtained a linear relationship between the pixel number corresponding to the peak of each Gaussian and the scanned angle of the PSD, yielding a value of 0.02213° ± 0.00007° per pixel relative to the sample position (0.475 mm between two adjacent pixels).

During data reduction, we first converted each pixel position to 2θ and then corrected the measured intensity for the average pixel efficiency. Throughout the run, the efficiency of all the polarizing elements was monitored by measuring the four spin-dependent transmissions for the main beam. The initial instrumental flipping ratio was determined to be 34 (31) using the spin flipper before (after) the sample. These values were slightly lower than the value of 37 expected from the combined efficiencies of the individual elements. We attribute this difference to imperfect transport of the neutron spin. Using the measured time-dependent efficiency of the ^{3}He analyzer, the polarization efficiencies for the SM polarizer and two spin flippers were obtained using procedures described elsewhere.[35] Time-dependent polarization corrections were then applied to the raw PSD data and the data from different scans were added together (if appropriate). The data were then corrected for footprint effects,[33] which is necessary because the sample does not fully intercept the incident beam at the smallest scattering angles. We note that the instrumental background was quite small during these runs (<0.016 s^{-1} per pixel) relative to the scattered intensity. Correction for the instrumental background was thus neglected.

IV. ^{3}He/PSD EXPERIMENT

A. Sample characteristics

The patterned Co sample was prepared using x-ray lithography at the Center for Advanced Microstructures and Devices, Louisiana State University. It consists of a single Co layer of 1000 nm deposited on a silicon substrate. A photoresist mask was applied to the Co layer surface to etch away ≈20 μm by ≈20 μm sections of the Co layer, forming periodic rectangular holes ("antidots") in the Co layer. The edge-to-edge separation between the antidots is ≈20 μm.

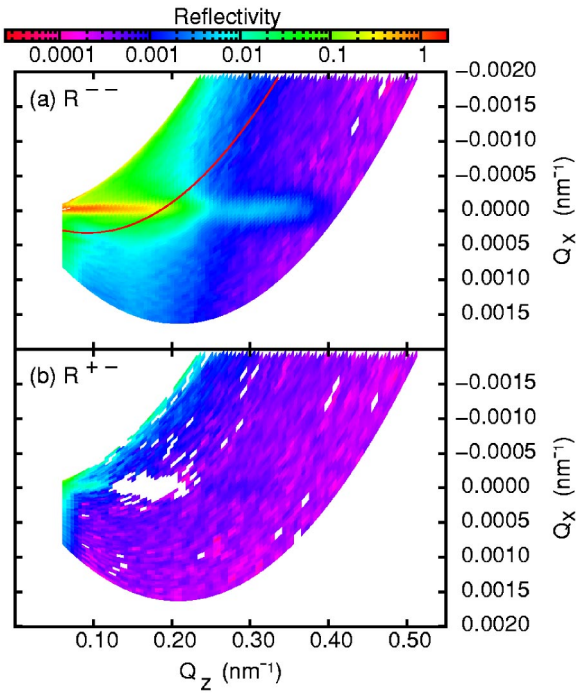

FIG. 3. (Color online) Two-dimensional Q_x-Q_z maps of reflectivities for the Co antidot sample: (a) R^{--} and (b) R^{+-} for the magnetized state (0.1 T). The absolute reflectivities shown have been corrected as described in the text. R^{++} and R^{-+} reflectivities are not shown here due to their similarity to R^{--} and R^{+-}, respectively. The red curve in Fig. 3(a) shows Q_x and Q_z for a fixed incident angle θ_i ($\theta_i=0.35°$). The white holes in Fig. 3 correspond to data points where a negative result occurs as a result of data reduction.

The magnetic field applied to the sample was provided by a custom, split-coil, water-cooled electromagnet with a maximum field of 700 mT.

B. Measurement geometry and comparison to the pencil ^{3}He detector

As shown in Fig. 2, the plane of the sample, one of the sides of an antidot, and the guide field were vertical (along the *y* axis). We measured all four reflectivities R^{++}, R^{+-}, R^{-+}, and R^{--} at each applied field value. R^{++} and R^{--} are nonspin-flip (NSF) reflectivities, which are sensitive to both the chemical structure and the projection of the in-plane magnetization parallel to the neutron polarization (applied field direction).[35] The difference between R^{++} and R^{--} is sensitive only to the in-plane magnetization parallel to the neutron polarization. R^{+-} and R^{-+} are spin-flip (SF) reflectivities, which are purely magnetic and sensitive to the in-plane magnetization perpendicular to the neutron polarization.[35] The wave vector transfers Q_x and Q_z [see *x* and *z* directions as shown in Fig. 2(a)] in the sample geometry can be expressed as a function of θ_i and θ_f

$$Q_x = \frac{2\pi}{\lambda}(\cos\theta_f - \cos\theta_i), \tag{1}$$

$$Q_z = \frac{2\pi}{\lambda}(\sin\theta_f + \sin\theta_i), \tag{2}$$

where λ is the neutron wavelength. These equations are useful in understanding the two-dimensional Q_x-Q_z map as discussed later. If $\theta_i=\theta_f$, then $Q_x=0$, which corresponds to specular scattering; All other scattering is off-specular scattering. Specular scattering provides a depth profile of the structure and magnetization (magnitude and orientation) averaged across the sample plane. Off-specular scattering for the antidot sample studied in this work arises from the artificial pattern of Co antidots and magnetic domains in the sample plane (see Sec. IV C).

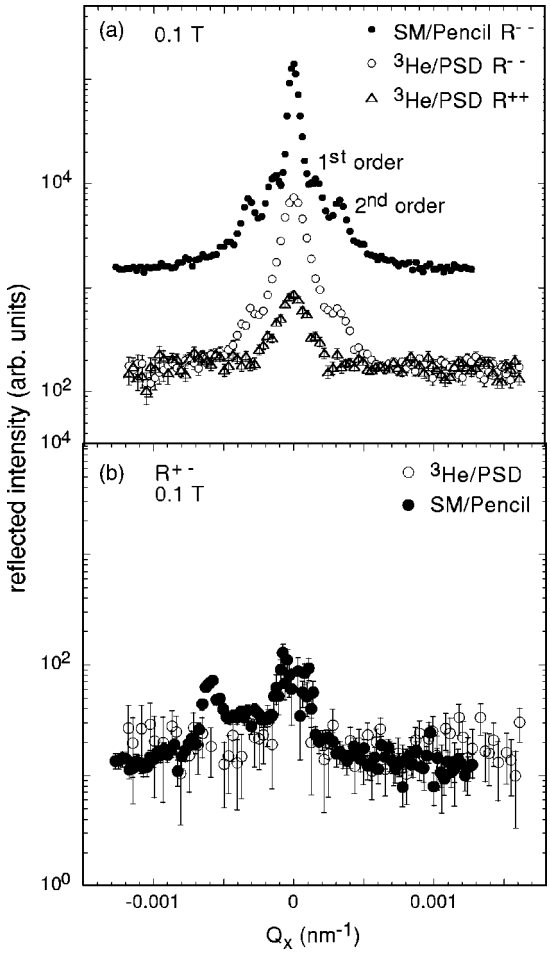

FIG. 4. Comparison of the reflected intensities obtained for $2\theta=0.77°$ ($Q_z \approx 0.178$ nm^{-1}): (a) R^{--} and (b) R^{+-} for a field of 0.1 T with the SM analyzer (filled circles) and the ^{3}He analyzer (open symbols). For the ^{3}He analyzer/PSD data, R^{++} (triangles) is also compared with R^{--} (circles). For clarity, the R^{--} data obtained with the SM/pencil detector configuration have been shifted up by an order of magnitude. We believe that the off-specular peak in the SM/pencil detector data for R^{+-} may be due to a spurious reflection. Comparison between the other two reflected intensities, R^{++} and R^{-+}, obtained with the SM analyzer/pencil detector and ^{3}He analyzer/PSD are in good agreement (not shown). The larger uncertainties for the R^{+-} data obtained with the ^{3}He analyzer/PSD configuration are due to a lower total number of counts.

PNR measurements were obtained first with the sample in a 0.1 T field applied parallel to the neutron polarization, which saturated the magnetization. For each incident angle θ_i, the reflectivity at a range of scattering angles 2θ was obtained from the PSD. By varying θ_i, a two-dimensional Q_x-Q_z map was constructed. The data, corrected for the polarizing efficiencies, are shown in Fig. 3 (color). Only R^{--} [Fig. 3(a)], and R^{+-} [Fig. 3(b)] reflectivities are shown here. The red curve in Fig. 3(a) shows Q_x vs Q_z plotted for a constant incident angle ($\theta_i=0.35°$). The white holes in Fig. 3

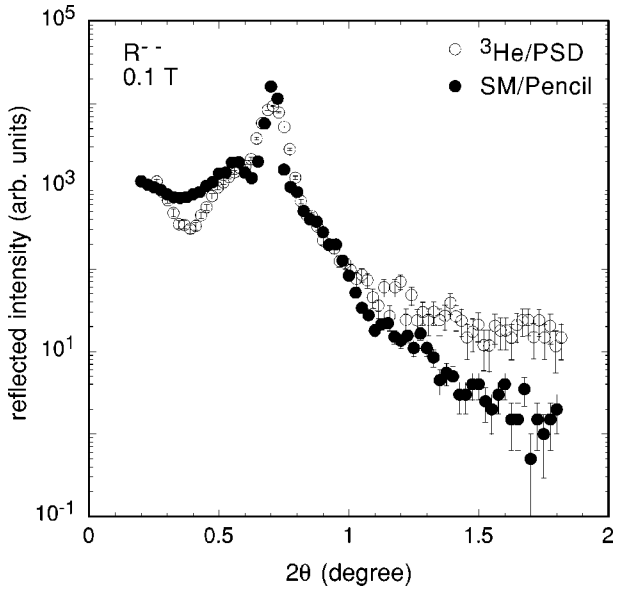

FIG. 5. Comparison of the R^{--} reflected intensity at $\theta_i=0.35°$ and at a field of 0.1 T: SM analyzer data (filled circles) and ^{3}He analyzer/PSD data (open circles). Comparison of the R^{++} reflected intensities (not shown here) is similar to that of the R^{--} reflected intensities. The higher intensities for the ^{3}He/PSD data at large scattering angles may be due to the background from the Plexiglas attenuator.

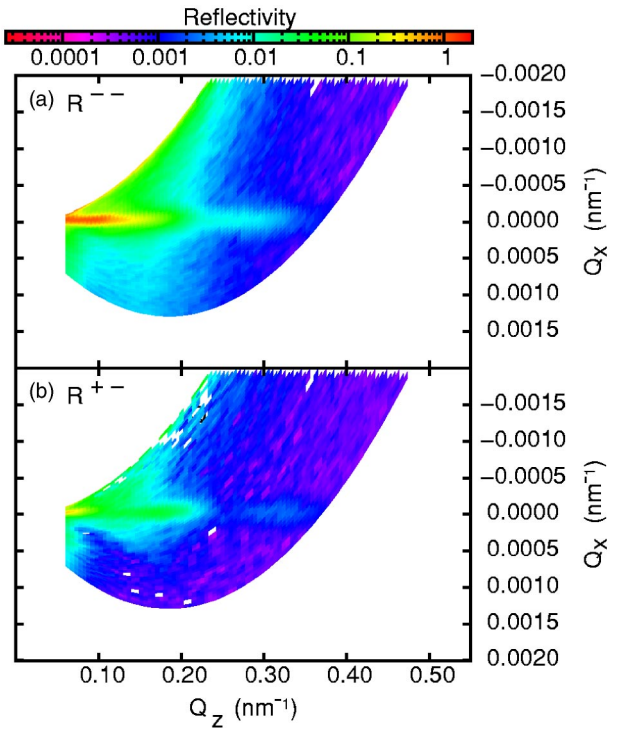

FIG. 6. (Color online) Two-dimensional Q_x-Q_z maps of reflectivities for the Co antidot sample: (a) R^{--} and (b) R^{+-} for the demagnetized state (zero applied field). The absolute reflectivities shown have been corrected as described in the text. R^{++} and R^{-+} reflectivities are not shown here due to their similiarity to R^{--} and R^{+-}, respectively. The white holes in Fig. 6 correspond to data points where a negative result occurs as a result of data reduction.

correspond to data points where a negative result occurs as a result of data reduction. The data in Fig. 3(b) generally fall within the uncertainties in our corrections, which are difficult to show in these two-dimensional color maps. The specular scattering is evident at $Q_x=0$.

To confirm our measurements obtained with the ^{3}He/PSD, we compared them to data obtained with the SM and pencil detector. We measured the scattered intensities with θ_i varied for a single scattering angle ($2\theta=\theta_i+\theta_f=0.77°$), and with the scattering angle varied for a single incident angle ($\theta_i=0.35°$). Figure 4 shows the reflected intensities R^{--} (a) and R^{+-} (b) for $2\theta=0.77°$ ($Q_z\approx0.178$ nm^{-1}) in a saturating field (0.1 T) measured with both the SM analyzer apparatus and the ^{3}He analyzer/PSD apparatus. Comparisons of the other two reflected intensities R^{++} and R^{-+} are not shown here. Accounting for the limited resolution of the PSD, the two sets of data show good agreement. The intensity modulation along Q_x in Fig. 4(a) originates from the periodic arrangement of artificial Co antidots across the sample plane as described before. Of particular significance is that the superlattice peak positions are the same in each data set. As expected, the SF reflected intensity was negligible [Fig. 4(b)]. The primary difference between the SM analyzer and the ^{3}He analyzer data is the resolution, which is much better for the SM configuration due to the use of collimating slits after the sample. We note the presence of the peak at $Q_x=-6\times10^{-4}$ nm^{-1} ($\theta_i=0.2°$). We believe this peak is possibly due to those scattered neutrons that hit the edge of the collimating slit and reach the detector. To account for differing numbers of counts for the SM/pencil detector and ^{3}He/PSD configurations, the data were scaled to make the background intensities equal. The larger uncertainties for the R^{+-} data obtained with the ^{3}He/PSD configuration are due to a lower total number of counts.

Figure 5 shows a plot of the R^{--} reflected intensity as a function of the scattering angle 2θ at a fixed θ_i of 0.35° in a field of 0.1 T. In this case neither Q_x nor Q_z is constant [for example, the red curve in Fig. 3(a)]. The good agreement between the data measured with the SM analyzer and the ^{3}He analyzer provides confidence for further application of the ^{3}He/PSD apparatus. For data taken with the ^{3}He analyzer/PSD configuration, a Plexiglas attenuator was placed just in front of the PSD to prevent the PSD from saturating. The higher intensities for the ^{3}He analyzer/PSD data at large scattering angles may be due to the background from the Plexiglas attenuator and/or the absence of the two collimating slits that were only used for the SM and the pencil detector configuration.

After removing the sample electromagnet, we demagnetized the Co antidot sample by immersing it in an oscillating magnetic field of decreasing magnitude. This was accomplished by simply alternating the orientation of a permanent magnet by hand, while slowly moving the magnet away from the sample. We measured the four reflectivities with the ^{3}He analyzer/PSD setup after the Co antidot sample was demagnetized and small guide field of 0.5 mT was applied on the sample. A two-dimensional Q_x-Q_z map is shown in Fig. 6 (color). The specular scattering is evident again at $Q_x=0$. Only R^{--} [Fig. 6(a)], and R^{+-} [Fig. 6(b)] reflectivities are shown here. Again, the white holes in Fig. 6 correspond to data points where a negative result occurs as a result of data reduction. In Fig. 7, the results are compared with those obtained from the fully magnetized state at $2\theta=0.77°$. As ex-

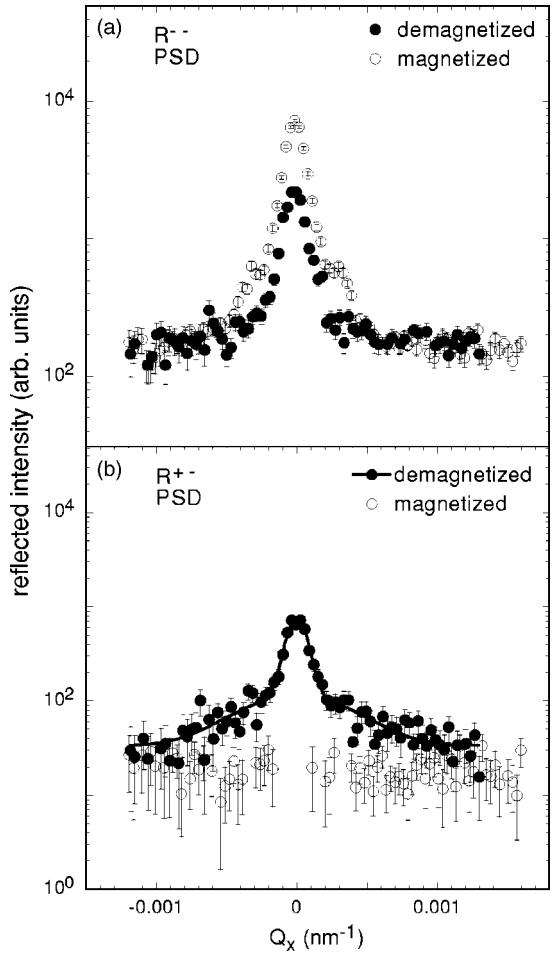

FIG. 7. Comparison of the reflected intensities measured with the ^{3}He analyzer/PSD system at $2\theta=0.77°$ ($Q_z\approx 0.178$ nm^{-1}): (a) R^{--} and (b) R^{+-} for the magnetized state (open circles) and the demagnetized state (filled circles). The solid line in Fig. 7(b) is a double Gaussian fit to the R^{+-} data in the demagnetized state, which yields an estimate of the magnetic domain size.

pected, the SF scattering intensities are stronger in the demagnetized state than in the fully magnetized state.

C. Results and interpretation

In a 0.1 T field, the sample is fully magnetized. The R^{--} reflected intensity is much stronger than R^{++} [Fig. 4(a)], whereas the SF reflected intensity was negligible [Fig. 4(b)]. These results indicate that almost all spins are aligned in the sample plane parallel to the applied field. The periodic array of Co antidots gives rise to off-specular superlattice peaks. These peaks are superimposed on the broad, diffuse scattering background that originates presumably from roughness and domains. These satellite peaks allow the determination of the lateral periodicity d by the simple relation $d=2\pi/Q_x$. The in-plane periodicity is determined to be 40 μm from the data in Fig. 4(a), consistent with the separation distance of 40 μm between the centers of two adjacent antidots determined from the film growth. We note that a patterned sample with holes 20 μm wide and 40 μm center-to-center separation, oriented along either the [01] or the [10] direction, should yield an interference pattern with a missing second order peak. The presence of the second order peak shown in Fig. 4(a) may indicate oxidation of the sample during long-term storage, which could result in a change of the antidot size (for example, a 30% increase in the antidot size is required to distinguish the second order peak from background).

When the sample is in the demagnetized state, there is no significant difference between the R^{++} (not shown here) and R^{--} NSF reflected intensities, implying the absence of any net magnetization parallel to the guide field. As shown in Fig. 7(b), we observed significant SF scattering in the demagnetized state compared to that in the fully magnetized state. No superlattice peaks can be discerned in the off-specular NSF scattering in the demagnetized state [Fig. 7(a)]. Magnetic disorder due to in-plane magnetic domains and the uniform magnetization of interlayers with rough interfaces (magnetic roughness) could yield a broad diffuse scattering peak.[15] The inverse of the FWHM of the magnetic diffuse peak is approximately equal to the in-plane coherence length.[15] Since the R^{-+} and R^{+-} SF scattering are purely magnetic, the in-plane coherence length is probably equivalent to the size of in-plane magnetic domains. Fitting the R^{+-} data as shown in Fig. 7(b) to a double Gaussian to obtain the FWHM of the broader peak provides an estimate of 6 μm for the magnetic domains in the demagnetized state. These domains are smaller than the separation distance between the adjacent antidots, consistent with microscopy results for $Ni_{80}Fe_{20}$ antidots in remanence.[36] Our results provide insights into the demagnetization process for these antidot structures.

In summary, we have polarization-analyzed specular and off-specular scattering at a broad range of angles simultaneously, using a polarized ^{3}He analyzer in conjunction with a PSD. The ^{3}He/PSD system is useful for a survey map of reciprocal space, allowing rapid determination of regions with pronounced off-specular scattering. The combination of a polarized ^{3}He analyzer and a PSD is efficient for probing in-plane structures and magnetic domains from $\sim$0.1 to $\approx$40 μm and layer thicknesses from 1 to 1000 nm. By operating the ^{3}He analyzer as a polarizer, the analyzing efficiency of the ^{3}He spin filter and its time dependence were determined independently of other elements in the polarized beam. The polarization declines on a time scale of several hundred hours because of the nearly complete suppression of wall relaxation in sealed spin-exchange optical pumping cells. This time scale is appropriate for time required for complete reflectivity characterization of a sample. In addition, SEOP will be convenient for future continuous optical pumping of a ^{3}He analyzer on a beamline.

ACKNOWLEDGMENTS

The authors thank J. Anderson and J. Fuller of the NIST Optical Shop for assistance with cell fabrication. They thank J. Barker for his great assistance in doing SANS measurements. The Co antidot sample was provided by Professor S. Adenwalla, University of Nebraska, and this is gratefully acknowledged. We also acknowledge the contributions of Andrew Lee, David Guccia, and Philip Gruber to the apparatus for measuring magnetic field gradients and development and

testing of the short shielded solenoid. The work at NIST was partially supported by Department of Energy Interagency Agreement No. DE-AI02-00ER45814.

[1] R. L. White, R. M. H. New, and R. F. W. Pease, IEEE Trans. Magn. **33**, 990 (1997).
[2] R. P. Cowburn, A. O. Adeyeye, and J. A. C. Bland, Appl. Phys. Lett. **70**, 2309 (1997).
[3] G. P. Felcher *et al.*, Rev. Sci. Instrum. **58**, 609 (1987).
[4] M. R. Fitzsimmons *et al.*, J. Magn. Magn. Mater. **271**, 46 (2004).
[5] C. F. Majkrzak, V. Nunez, J. R. D. Copley, J. F. Anker, and G. C. Greene, in *Neutron Optical Devices and Applications, SPIE Proc. Vol. 1738*, edited by C. F. Majkrzak and J. Wood (SPIE, Bellingham, WA, 1992), p. 90 and references therein.
[6] C. F. Majkrzak, Physica B **213**, **214**, 904 (1995).
[7] T. Krist, H. Fritzsche, and F. Mezei, Appl. Phys. A: Mater. Sci. Process. **74**[Suppl.], S221 (2002).
[8] http://www.ill. fr/YellowBook/D7.
[9] T. R. Gentile *et al.*, J. Appl. Crystallogr. **33**, 771 (2000).
[10] B. Nickel *et al.*, Rev. Sci. Instrum. **72**, 163 (2001).
[11] F. Radu *et al.*, Physica B **335**, 63 (2003).
[12] W. Heil *et al.*, Nucl. Instrum. Methods Phys. Res. A **485**, 551 (2002).
[13] S. K. Sinha, E. B. Sirota, S. Garoff, and H. B. Stanley, Phys. Rev. B **38**, 2297 (1988).
[14] D. E. Savage *et al.*, J. Appl. Phys. **69**, 1411 (1991).
[15] S. K. Sinha, in *Neutron Scattering in Materials Science II*, edited by D. A. Neumann, T. P. Russel, and B. J. Wuensch, Mater Res. Soc. Symposium Proceedings (Materials Research Society, Pittsburg, 1995), Vol. 376, p. 175.
[16] J. A. Borchers *et al.*, Physica B **283**, 162 (2000); J. A. Borchers *et al.*, Phys. Rev. Lett. **82**, 2796 (1999).
[17] S. Langridge, J. Schmalian, C. H. Marrows, D. T. Dekadjevi, and B. J. Hicky, Phys. Rev. Lett. **85**, 4964 (2000).
[18] F. D. Colegrove, L. D. Schearer, and G. K. Walters, Phys. Rev. **132**, 2561 (1963), and references therein.
[19] T. G. Walker and W. Happer, Rev. Mod. Phys. **69**, 629 (1997).
[20] D. R. Rich *et al.*, Appl. Phys. Lett. **80**, 2210 (2002).
[21] B. Chann *et al.*, J. Appl. Phys. **94**, 6908 (2003).
[22] W. C. Chen *et al.*, Physica B **335**, 196 (2003).
[23] B. Chann, I. Nelson, and T. G. Walker, Opt. Lett. **25**, 1352 (2000).
[24] B. Chann, E. Babcock, L. W. Anderson, and T. G. Walker, Phys. Rev. A **66**, 032703 (2002).
[25] W. G. Williams, *Polarized Neutrons* (Oxford University Press, New York, 1988), p. 135.
[26] GE Lighting Component Sales, Cleveland, OH 44117. Certain trade names and company products are mentioned in the text or identified in an illustration in order to adequately specify the experimental procedure and equipment used. In no case does such identification imply recommendation or endorsement by the National Institute of Standards and Technology, nor does it imply that the products are necessarily the best available for the purpose.
[27] C. J. Glinka *et al.*, J. Appl. Crystallogr. **31**, 430 (1998); http://www.ncnr.nist.gov/instruments/ng7sans/.
[28] G. L. Jones *et al.*, Nucl. Instrum. Methods Phys. Res. A **440**, 772 (2000).
[29] N. R. Newbury *et al.*, Phys. Rev. A **48**, 4411 (1993).
[30] L. D. Schearer and G. K. Walters, Phys. Rev. **139**, A1398 (1965).
[31] E. Stoltz *et al.*, Appl. Phys. B: Lasers Opt. **63**, 629 (1996).
[32] E. Stoltz, B. Villard, M. Meyerhof, and P. J. Nacher, Appl. Phys. B: Lasers Opt. **63**, 635 (1996).
[33] K. V. O'Donovan, J. A. Borchers, C. F. Majkrzak, O. Hellwig, and E. E. Fullerton, Phys. Rev. Lett. **88**, 067201 (2002); http://www.ncnr.nist.gov./instruments/ng1refl/.
[34] C. F. Majkrzak, D. A. Neumann, J. R. D. Copley, and R. P. DiNardo, Proceeding of the 1987 Fall Meeting of the Materials Research Society, 1987, Vol. 103, p. 115 (unpublished).
[35] C. F. Majkrzak, Physica B **221**, 342 (1996).
[36] A. Yu. Toporov, R. M. Langford, and A. K. Petford-Long, Appl. Phys. Lett. **77**, 3063 (2000).